Hindawi
International Journal of Antennas and Propagation
Volume 2019, Article ID 9479010, 9 pages
https://doi.org/10.1155/2019/9479010

*Research Article*

# A Single-Layer Dual-Band Reflectarray Cell for 5G Communication Systems

**Sandra Costanzo, Francesca Venneri, Antonio Borgia, and Giuseppe Di Massa**

*Università della Calabria, Rende, Italy*

Correspondence should be addressed to Sandra Costanzo; costanzo@dimes.unical.it

Received 29 August 2018; Revised 18 December 2018; Accepted 14 January 2019; Published 11 March 2019

Guest Editor: Khalil Sayidmarie



A single-layer dual-band reflectarray cell is proposed in this work for future 5G systems. A reflectarray unit cell operating at 28/38 GHz is designed by adopting two pairs of miniaturized fractal patches, offering low losses (<0.7 dB) and almost full-phase ranges (≅320°) at both operating frequencies. The proposed configuration allows to achieve very small interelement spacings and negligible mutual coupling effects between the two bands, thus assuring an independent phase-tuning mechanism at both desired frequency bands. The designed compact cell is successfully adopted to demonstrate reflectarrays' abilities in achieving fixed scanned-beam and/or multibeam patterns, under the dual-band operation mode. Full-wave numerical validations, performed on the synthesized reflectarray structures, confirm the effectiveness of the designed dual-band configuration in achieving independent radiation patterns and quite good bandwidths, at the two designed frequencies. Thanks to its compactness and versatility in achieving both frequency diversity and multibeam/scanned-beam radiation patterns, the proposed unit cell is appealing for future 5G applications.

## 1. Introduction

Nowadays, the development of new technologies for future fifth generation (5G) wireless communication networks is the main challenge in the telecommunications industry. 5G communication systems are expected to meet the growing demand for higher data rates (i.e., 1-10 theoretically gigabit per second (Gbps) [1]), as required by multimedia applications and the Internet of Things (IoT). To address this demand, 5G systems will use millimeter wave (mmw) frequencies, which represent one of the key enabling technologies in the development and implementation of 5G communication networks [1, 2]. However, the mmw frequencies are characterized by propagation limitations, such as higher path loss and shorter communication distances, mainly due to the atmospheric absorption of electromagnetic waves at higher frequencies [3]. For this reason, there is a need for designing high-gain antennas able to compensate for path losses. To this end, microstrip array antennas may represent a good candidate, providing also a narrow beamwidth and very thin profiles that are essential for 5G operations. Some interesting 5G array antennas have been recently proposed in [2, 4, 5].

A very attractive alternative solution for designing 5G antennas is offered by microstrip reflectarrays [6, 7]. They consist of an array of microstrip elements illuminated by a feed antenna. Each element is designed to compensate for the phase delay in the path coming from the feed and to introduce a phase contribution giving a prescribed main beam direction in the antenna radiation pattern. Thanks to their higher efficiencies, due to the adopted spatial feeding approach [6], reflectarrays represent a promising solution for designing high-gain/directivity 5G antennas. Furthermore, reflectarrays can be properly designed to offer several reconfiguration capabilities, which are very appealing for 5G systems [2], such as beam-steering functions and/or frequency agility [6, 8–11], multibeam radiation patterns [6, 9], and multiband operation modes [6].

In order to demonstrate reflectarray versatility in satisfying most of the 5G requirements, a single-layer dual-band reflectarray cell is investigated in this paper to operate within the Ka band (at 28/38 GHz), which is currently under

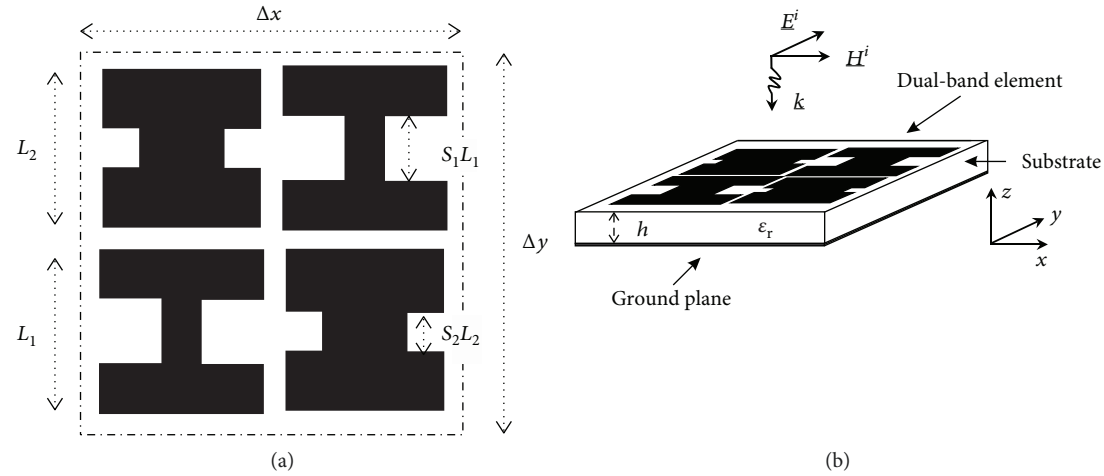


Figure 1: Unit cell layout: (a) top view and (b) 3D view and reference system.

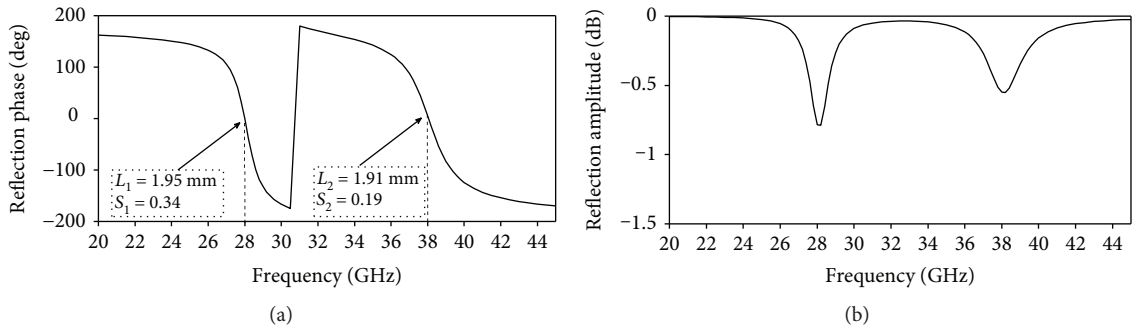


Figure 2: Simulated unit cell reflection coefficient vs. frequency: (a) phase and (b) amplitude.

consideration for 5G technologies [2]. The proposed cell is adopted to demonstrate reflectarrays' abilities in achieving fixed scanned-beam and/or multibeam patterns, under the dual-band operation mode.

The fractal concept has yet to be applied in the literature to reflectarray antennas, as reported in [12–16]. In this paper, a modified layout of the fractal element, originally proposed by the authors in [12, 13], is investigated to design a compact single-layer dual-band cell with single linear polarization, offering low losses (<0.7 dB) and almost full-phase ranges (≅320°), at both operating frequencies. The miniaturization capabilities of the adopted fractal geometry are exploited to achieve a dual-band behavior, simply by embedding two pairs of miniaturized resonators within the same unit cell. Negligible mutual effects between the two bands are demonstrated, thus achieving an independent phase-tuning mechanism for each frequency band, by properly changing the fractal shapes. Unlike other multiband reflectarray cells presented in the literature [17–21], the proposed dual-band fractal cell allows to achieve the following: a simpler and thinner structure with respect to the multilayer stacked configurations [17, 18]; smaller unit cell size at both operating frequencies (≅0.4$\lambda$ at 28 GHz, ≅0.54$\lambda$ at 38 GHz) with respect to other single-layer configurations [19, 20], thus preserving the capability to point the main beam at large scan angles, without occurring in grating lobe phenomena; and smaller electrical interferences between the elements operating at the different bands [21], despite the adopted small interelement spacing.

As a first proof of the concept, the proposed cell is adopted to design reflectarrays able to independently scan the main beam at the two operating frequencies. A 1 dB gain-bandwidth of about 1 GHz is simulated at both operating frequencies, potentially offering several Gbps of data rates at 28 or 38 GHz [1]. Moreover, a dual-band multibeam reflectarray design is numerically demonstrated. Finally, the dual-band behavior of the proposed unit cell configuration is experimentally validated.

## 2. Dual-Band Reflectarray Unit Cell

The proposed dual-band unit cell is composed of two alternately arranged pairs of fractal patches (Figure 1), each designed to operate around a specific resonant frequency. The layout of the single patch is essentially derived from the 1st iteration fixed-length Minkowski patch originally proposed by the authors in [12]. The patch geometry, reported in Figure 1(a), is characterized by a beginning of dimensions $L_n \times L_n$ ($n = 1, 2$). A smaller square of the side $S_nL_n$ is removed from the center of the two lateral sides (i.e., the resonant sides), thus obtaining a linearly polarized

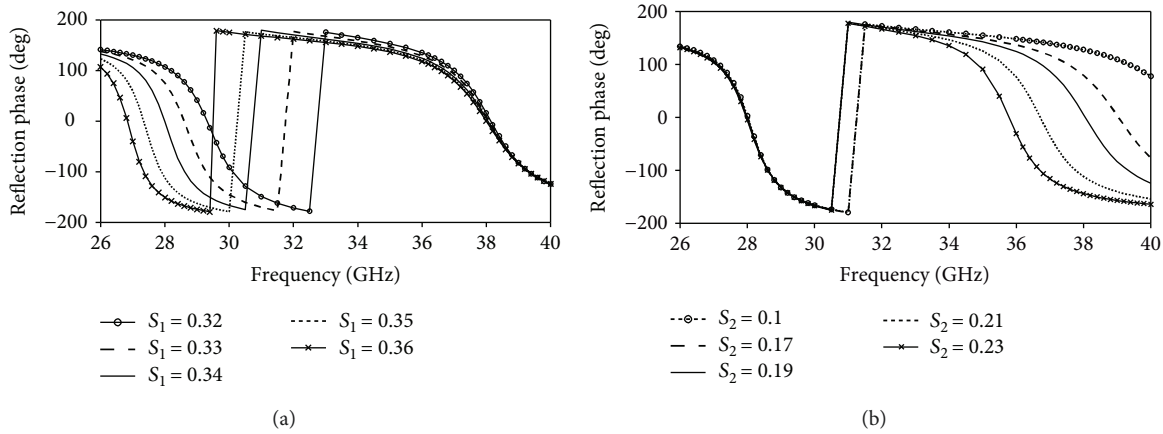


Figure 3: Simulated unit cell reflection coefficient vs. frequency for different scaling factors: (a) $L_1 = 1.95$ mm, $S_1$ = variable and $L_2 = 1.91$ mm, $S_2 = 0.19$; (b) $L_1 = 1.95$ mm, $S_1 = 0.34$ and $L_2 = 1.91$ mm, $S_2$ = variable.

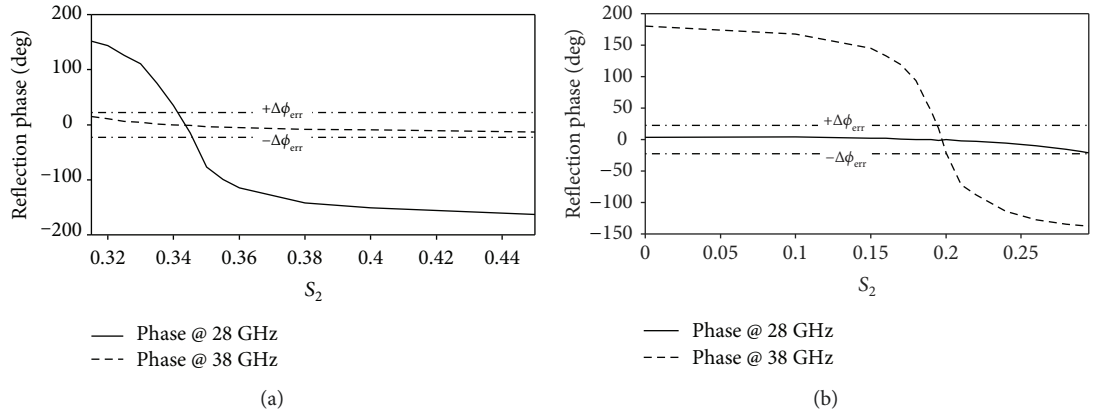


Figure 4: Simulated phase curve vs. the scaling factors $S_1$ and $S_2$, at the two operating frequencies: (a) $L_1 = 1.95$ mm, $S_1$ = variable and $L_2 = 1.91$ mm, $S_2 = 0.19$; (b) $L_1 = 1.95$ mm, $S_1 = 0.34$ and $L_2 = 1.91$ mm, $S_2$ = variable.

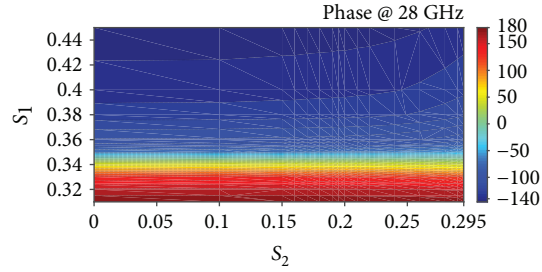


Figure 5: Simulated reflection phase vs. $S_1$ and $S_2$ (at 28 GHz).

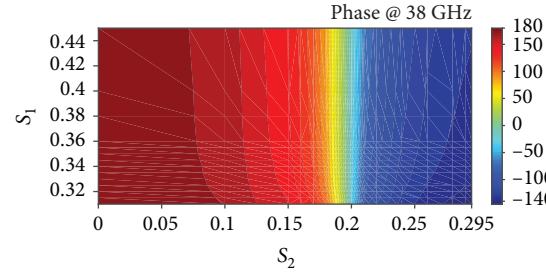


Figure 6: Simulated reflection phase vs. $S_1$ and $S_2$ (at 38 GHz).

element, along the $y$-axis (Figure 1(b)). The scaling factor $S_n$ varies from 0 up to 0.45. The reflection phase tuning is realized by independently varying the fractal scaling factor $S_n$ of each element, leaving unchanged the patch size $L_n \times L_n$. The above fractal shape allows to fit a longer electrical resonator into a smaller unit cell [12], thus offering very appealing miniaturization skills. Furthermore, the fixed length of the radiating sides (i.e., the upper and lower sides of the patch in Figure 1(a)) guarantees a higher independence to mutual coupling effects. As a matter of fact, in [22], it is demonstrated how the stronger contribution to the mutual coupling between microstrip patches is that occurring along the $E$-plane ($yz$-plane in Figure 1(b)).

*2.1. Unit Cell Design.* The layout depicted in Figure 1 is adopted to design a dual-band unit cell operating at the following 5G frequencies: $f_1 = 28$ GHz and $f_2 = 38$ GHz. A benzocyclobutene (BCB) polymer is adopted as a substrate material. The excellent material features in terms of low loss

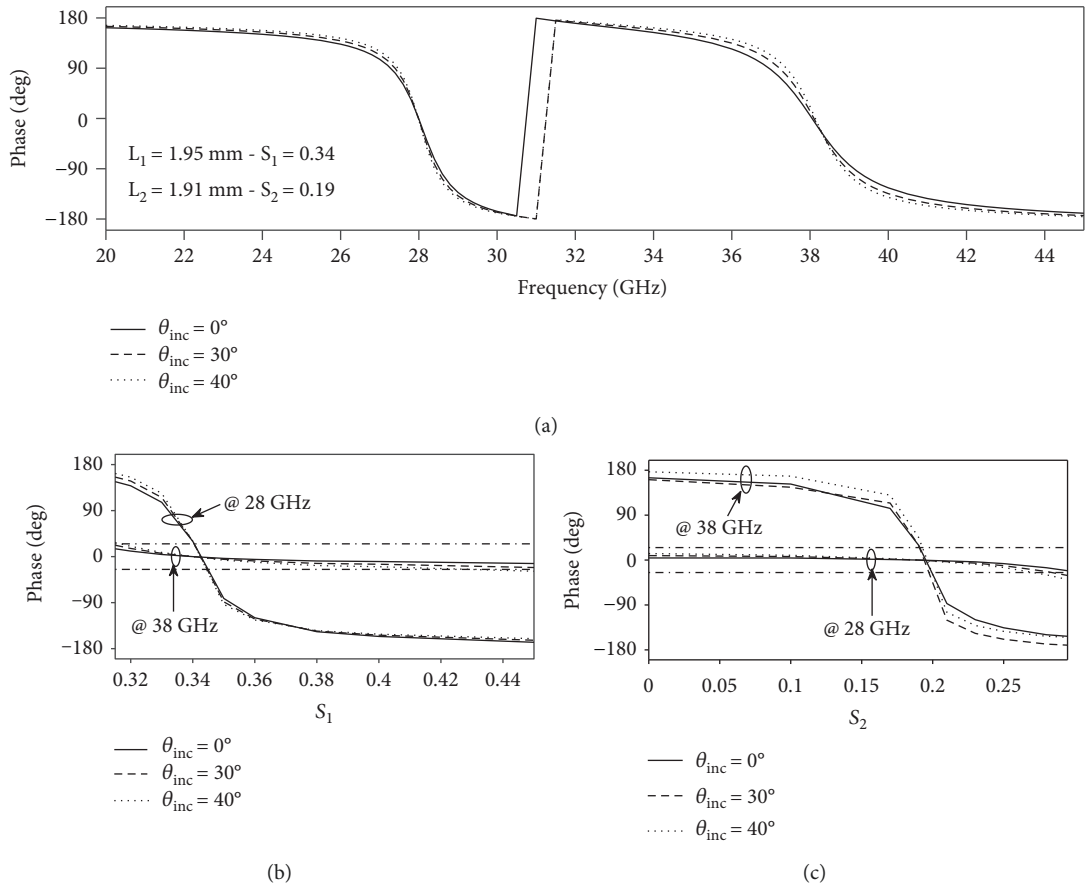


Figure 7: Simulated reflection phase curves for different incidence angles: (a) phase vs. frequency; (b) phase vs. the scaling factor $S_1$ at the two operating frequencies ($L_1 = 1.95$ mm, $S_1$ = variable and $L_2 = 1.91$ mm, $S_2 = 0.19$); (c) phase vs. the scaling factor $S_2$ at the two operating frequencies ($L_1 = 1.95$ mm, $S_1 = 0.34$ and $L_2 = 1.91$ mm, $S_2$ = variable).

(tan $\delta \leq 0.008$), low dielectric constant (≅2.65), and strong dielectric stability against frequency and temperature make the BCB polymer a good choice for designing mmw microstrip antennas [23, 24]. A substrate thickness equal to 0.26 mm is fixed [24]. A commercial full-wave code [25], based on the infinite array approach, is adopted for unit cell analysis. A normal incident plane wave is considered ($\theta_{inc} = 0°$). A periodicity of 4.3 mm is fixed in both directions (i.e., $\Delta x = \Delta y = 4.3$ mm) corresponding to $0.4\lambda$ at 28 GHz and $0.54\lambda$ at 38 GHz. Following the design rules outlined in [12], the unit cell is designed to achieve the desired dual-resonant behavior. In particular, remembering that the use of smaller patch lengths $L_n$ gives higher resonant frequencies and, conversely, the use of greater $S_n$ values allows to move down the resonant frequencies, the size of the fractal patches is fixed to the values depicted in Figure 2. The minimum distance between two adjacent elements (i.e., $(\Delta x - L_1 - L_2)/2 = (\Delta y - L_1 - L_2)/2$, see Figure 1) is equal to 0.22 mm. Both the phase (Figure 2(a)) and the amplitude (Figure 2(b)) of the unit cell reflection coefficient are illustrated in Figure 2. Similar phase curve behavior vs. frequency can be observed at both resonances (Figure 2(a)). Furthermore, low losses smaller than 0.7 dB can be appreciated in Figure 2(b).

*2.2. Parametric Analysis of the Unit Cell.* The reflection phase tuning is independently realized at each resonant frequency $f_n$, by varying the corresponding fractal scaling factor $S_n$, leaving unchanged the patch size $L_n \times L_n$. Both factors, $S_1$ and $S_2$, are properly tuned to achieve a full-phase tuning range, at the corresponding operating frequency. Figure 3 shows the effectiveness of the adopted phase-tuning mechanism that allows to independently vary the reflection phase at each desired frequency. In particular, it can be observed that, by changing the scaling factor $S_1$ associated to the 28 GHz resonant element and leaving unchanged the other fractal sizes, the phase response of the unit cell varies only corresponding to a neighborhood of $f_1 = 28$ GHz, whilst a negligible phase variation is obtained at $f_2 = 38$ GHz (Figure 3(a)). A similar behavior can be observed in Figure 3(b). In fact, by varying the scaling factor $S_2$, a variable phase shift is introduced only corresponding to a neighborhood of $f_2 = 38$ GHz, leaving unchanged the phase response at $f_1 = 28$ GHz. The phase curves computed vs. the scaling factors $S_n$ (Figure 4) show the admissible scaling factor variation range for both $S_1$ (Figure 4(a)) and $S_2$ (Figure 4(b)). In other words, the results depicted in Figure 4 affirm that, in order to achieve a quite full-phase tuning range (≅320°) at 28 GHz, the scaling

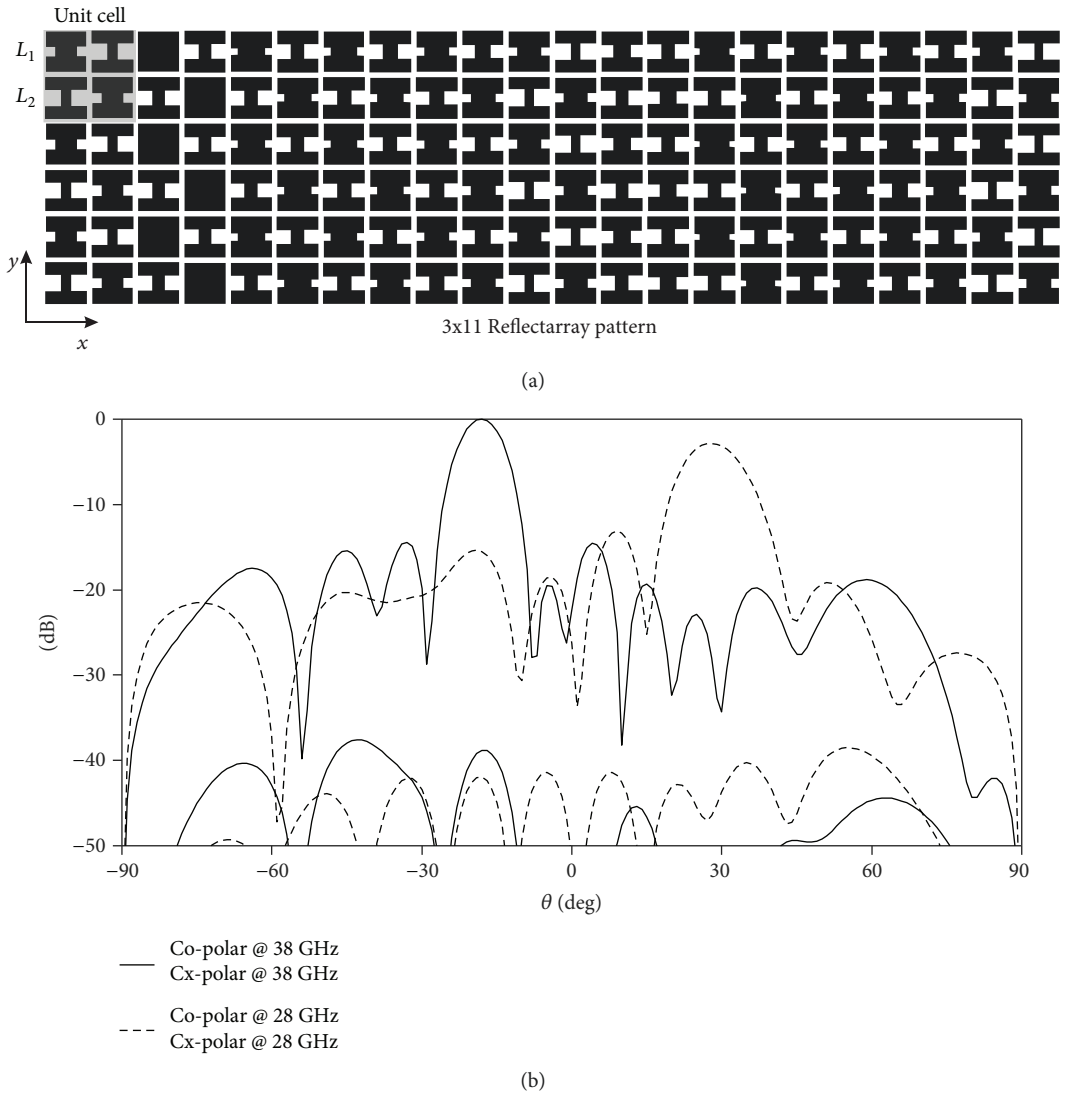


FIGURE 8: Synthesized dual-band scanned reflectarray: (a) reflectarray layout and (b) simulated radiation patterns at the designed frequencies.

factor $S_1$ must be varied from 0.31 up to 0.45, assuring also small phase excursions, corresponding to the frequency $f_2 = 38$ GHz, that are comprised between the phase error margins given by $\pm\Delta\phi_{\text{err}} = \pm 22.5^\circ$ (Figure 4(a)). Conversely, the scaling factor $S_2$ must be varied within the value range starting from 0 up to 0.29, in order to assure a quite full-phase range at 38 GHz and a confined phase excursion error corresponding to the frequency $f_1 = 28$ GHz (Figure 4(b)).

In order to give a more exhaustive description of the reflection phase response computed for the designed dual-band unit cell, a contour plot is reported under Figures 5 and 6, showing, respectively, the phase variations computed at frequency $f_1 = 28$ GHz vs. $S_1$, for different $S_2$ values (Figure 5), and the phase computed at frequency $f_2 = 38$ GHz vs. $S_2$, for different $S_1$ values (Figure 6). Both figures confirm how the proposed dual-band unit cell can offer an independent phase-tuning mechanism at each designed frequency band. As a matter of fact, a quite constant reflection phase can be observed at 28 GHz (Figure 5), by changing the scaling factor $S_2$ for a fixed $S_1$ value. Similar considerations can be extrapolated from Figure 6.

The unit cell is further analyzed to investigate the behavior of its phase response, for different incidence angles of the impinging wave. Figure 7 shows acceptable phase variations under 30° and 40° oblique incidence angles, with respect to the normal case. Furthermore, as depicted in Figures 7(b) and 7(c), the independency of the phase-tuning mechanism is preserved at both frequencies also in the case of oblique incidence angles. In particular, it can be observed that, by changing the scaling factor $S_1$ associated to the 28 GHz resonant element, negligible phase variations are obtained at the frequency $f_2 = 38$ GHz (Figure 7(a)). A similar behavior can be observed in Figure 7(b), in the case of the 38 GHz resonant patch.

## 3. Dual-Band Reflectarray Designs

In order to prove the effectiveness of the proposed dual-band unit cell, two small $3 \times 11$ reflectarray designs

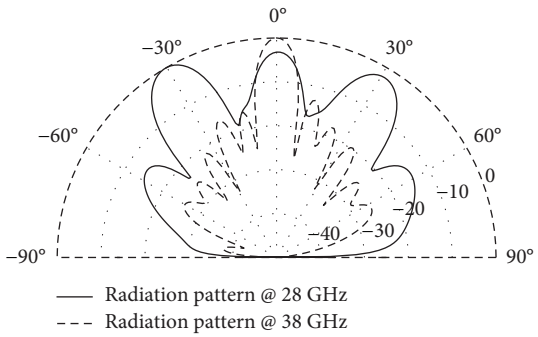


Figure 9: Synthesized dual-band multibeam reflectarray: simulated radiation patterns at the designed frequencies.

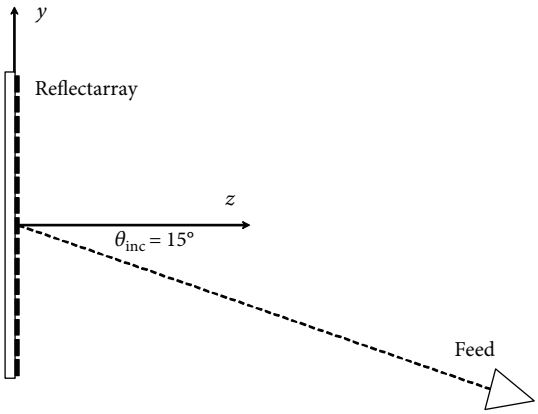


Figure 10: Schematic layout of the 15 × 15 reflectarray.

are reported in the following. The high independence between the two designed frequency bands (28/38 GHz), demonstrated in Section 2.2, allows to separately synthesize the two sets of resonant fractal patches (identified by $L_1$ and $L_2$ in Figure 1), without affecting the accuracy of the adopted design procedure. Both reflectarrays are designed by adopting a synthesis algorithm [9] that receives as input the desired radiation pattern, in terms of the main beam direction and maximum side lobe level, and automatically returns the required excitation phase on each reflectarray cell. The algorithm uses the phase design curves depicted in Figures 4(a) and 4(b) that assume fixed fractal patch sizes, except the adopted phase-tuning parameter (i.e., $S_1$ for $f_1 = 28$ GHz and $S_2$ for $f_2 = 38$GHz). A normal incident plane wave is considered.

The first design consists of a reflectarray able to independently scan the main beam at the two different operating frequencies, whilst the second design is characterized by a multibeam pattern.

The fractal patches embedded in each cell of the first reflectarray are chosen as follows: the elements resonating within the 28 GHz band, identified by the couple ($L_1$, $S_1$), are computed giving the main lobe steered towards the direction $\theta_{MB} = 30°$, in the $H$-plane ($xz$-plane in Figure 8); whilst the elements resonating within the 38 GHz band, identified by ($L_2$, $S_2$), are chosen by imposing a main beam direction equal to -20°, in the $H$-plane. Figure 8 shows the synthesized

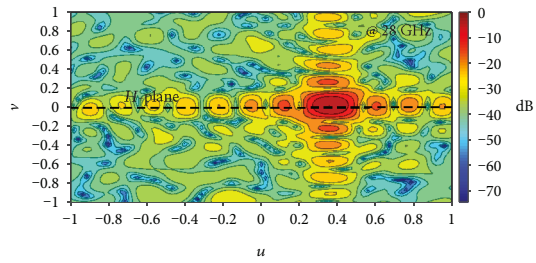


Figure 11: Synthesized 28 GHz pattern of the 15 × 15 offset-fed reflectarray.

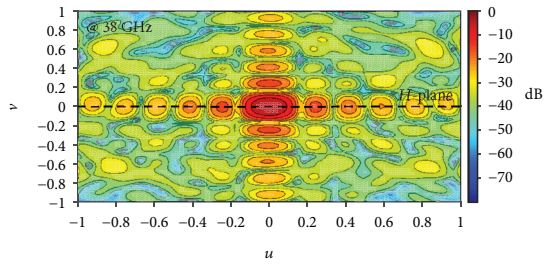


Figure 12: Synthesized 38 GHz pattern of the 15 × 15 offset-fed reflectarray.

reflectarray layout (Figure 8(a)) and the full-wave simulations of the overall structure. In particular, two independent radiation patterns are achieved at the two designed frequencies. Both patterns fully satisfy the constraints imposed during the synthesis stage, confirming the effectiveness of the proposed dual-band unit cell.

Furthermore, a dual-band 3 × 11 reflectarray is designed to achieve a multibeam radiation pattern corresponding to the first resonance (i.e., 28 GHz). In particular, a pattern having three beams, respectively, directed along -30°, 0°, and 30° in the $H$-plane, is synthesized at 28 GHz, whilst a broadside radiation pattern is imposed at 38 GHz. The full-wave simulation of the overall reflectarray structure is depicted in Figure 9. The simulated patterns match quite well the constraints imposed during the synthesis stage.

Finally, a 15 × 15 reflectarray is designed to independently direct the main lobes at the two different operating frequencies in the $H$-plane (i.e., $\theta_{MB} = 20°$ at 28 GHz and $\theta_{MB} = 0°$ at 38 GHz). The reflecting surface is illuminated by a Ka-band horn (characterized by a 15 dB gain and a 16.6 mm × 20.2 mm aperture), which is placed in the $E$-plane (i.e., the $yz$-plane in Figure 10), at a distance of 16.5 cm from the reflecting surface, with an offset angle of about 15°. The two couples of elements are properly synthesized to compensate the phase delay in the paths from the feed and to introduce a proper phase contribution able to meet the synthesis constraints. Figures 11 and 12 show the contour plot of the synthesized patterns in $u$-$v$ coordinates, where $u = \sin(\theta)\cos(\phi)$ and $v = \sin(\theta)\sin(\phi)$. Figure 13 illustrates the gain patterns vs. frequency, computed, respectively, along the main beam direction $(\theta_{MB}, \phi_{MB}) = (20°, 0°)$, in the case of the 28 GHz radiation pattern, and along the direction $(\theta_{MB}, \phi_{MB}) = (0°, 0°)$, in the case of

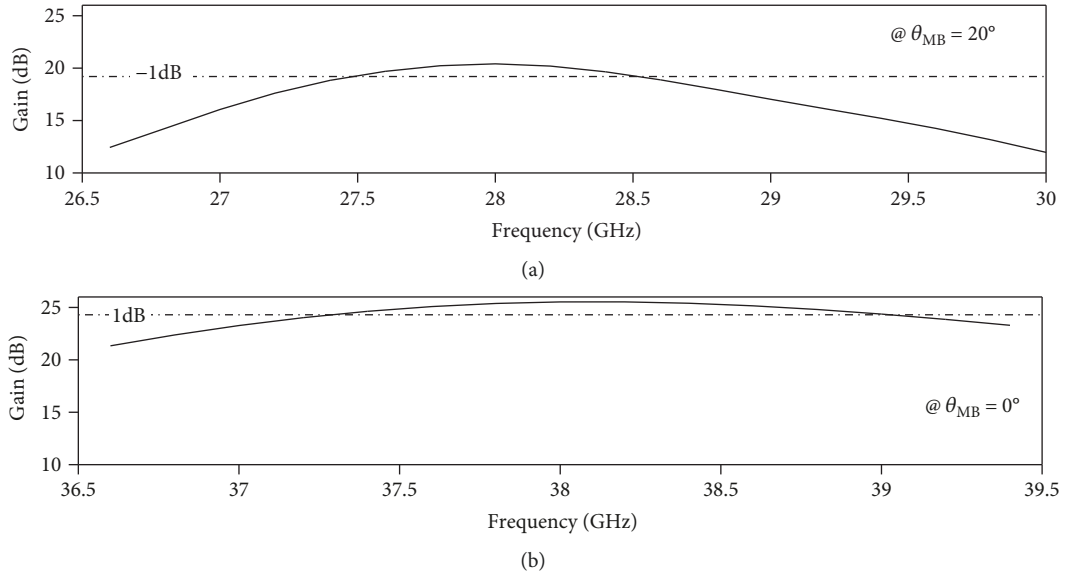


Figure 13: Simulated gain pattern versus frequency in the $H$-plane: (a) $\theta = 20^\circ$ and (b) $\theta = 0^\circ$.

the 38 GHz radiation pattern. A greater gain peak value can be observed in the case of the 38 GHz pattern (i.e., the gain difference is about 4.2 dB), mainly due to the greater electrical size and the lower spillover characterizing the antenna aperture at the higher operating frequency (38 GHz) and secondly due to lower scan losses [26]. Although the structures have not been properly optimized in terms of bandwidth, the simulated gain patterns show an acceptable 1 dB gain-bandwidth, approximately equal to 950 MHz at 28 GHz (≅3.4%) and to 1.5 GHz at 38 GHz (≅3.9%), that, at the considered mmw frequencies, can potentially offer high data rates [1], as required by 5G applications.

The above reflectarray designs confirm the effectiveness of the proposed dual-band unit cell in achieving an independent control of the reflectarray radiation features at each operating frequency. As future developments, the proposed configuration will be further optimized in terms of bandwidth. Furthermore, experimental validations of the configuration will be scheduled in order to deal with the problems associated with the manufacturing process, such as fabrication tolerances and illumination feed displacement, not yet considered in this work.

## 4. Experimental Validation of the Unit Cell

In order to give a preliminary validation of the proposed dual-band unit cell, a small array prototype, composed of $11 \times 11$ identical cells, is realized and tested in the Microwave Laboratory of the University of Calabria (Figure 14). The array is printed on a DiClad 880 substrate, having $\varepsilon_r = 2.24$ and $h = 0.254$ mm [27]. A periodicity equal to 5 mm is fixed in both directions. The patches embedded in each unit cell are characterized by the following dimensions: $L_1 = 2.24$ mm, $S_1 = 0.33$ and $L_2 = 2.1$ mm, $S_2 = 0.2$, giving a minimum distance between two adjacent patches equal to about 0.33 mm. The cell operates in a dual-band mode corresponding to about 29 GHz and 39 GHz.

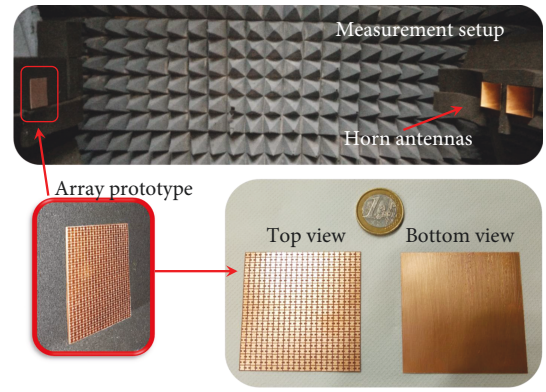


Figure 14: Reflection phase measurement setup and the dual-band array prototype.

A far-field measurement system is adopted (Figure 14), consisting of two identical transmitting and receiving horn antennas (operating within the $(26.5 \div 40)$ GHz frequency band), both connected to a vector network analyzer. The instrumentation detects the field reflected by the array along the broadside direction in the far-field region [9]. The reflection phase curve of the cell is measured within the frequency range $26.5 \div 40$ GHz (Figure 15). It can be observed a phase variation of about 300° around both operating frequencies. Furthermore, a good agreement between simulations and measurements can be observed in Figure 15, showing a small but appreciable frequency shift, mainly due to the fabrication error tolerance related to the adopted printed circuit board (PCB) milling process [28]. Anyway, the effects due to the above errors can be reduced through a proper reiteration of the unit cell synthesis procedure (see Section 2) or, alternatively, by adopting a more precise fabrication process, as that described in [23, 24]. In conclusion, it can be stated that the experimental results confirm the dual-band behavior of the proposed configuration.

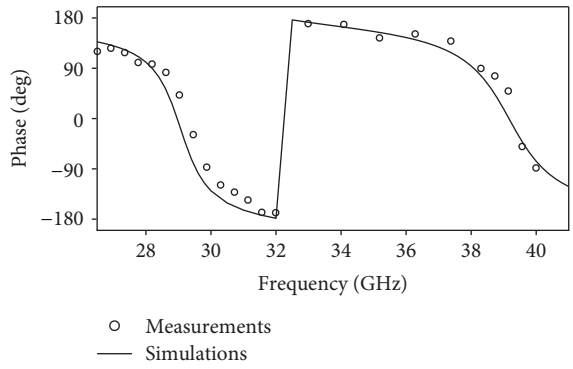


Figure 15: Comparison between measured and simulated phase curve vs. frequency.

## 5. Conclusion

A single-layer dual-band reflectarray with a single linear polarization cell has been investigated in this work for future 5G wireless communication networks. A reflectarray unit cell operating within the Ka band (at 28/38 GHz) has been designed. Two pairs of miniaturized fixed-length fractal patches have been synthesized, achieving low losses (<0.7 dB) and almost full-phase ranges (≅320°), at both operating frequencies. A thorough parametric analysis of the unit cell has been performed, demonstrating negligible mutual coupling effects between the two pairs of resonant elements, so assuring the independence between the two designed frequency bands. The designed compact cell has been successfully adopted to demonstrate reflectarrays' abilities in achieving fixed scanned-beam and/or multibeam patterns, under the dual-band operation mode.

Full-wave simulations of the synthesized reflectarray structures have been performed, confirming the effectiveness of the designed dual-band configuration in achieving independent radiation patterns at the two designed frequencies. In conclusion, the designed dual-band configuration offers, at the same time, compactness, low losses, frequency diversity, high versatility in achieving fixed scanned-beam and/or multibeam radiation patterns, and quite good gain-bandwidths. The above features make the proposed dual-band reflectarray configuration appealing for the implementation of 5G antennas. A preliminary experimental validation of the dual-band behavior of the proposed unit cell has been performed.

As future developments, the proposed configuration will be further optimized in terms of bandwidth and fabrication tolerances. Further experimental validations on dual-band reflectarray prototypes will be scheduled for the future, in order to give a comprehensive proof of the proposed concept.

## Data Availability

The data used to support the findings of this study are included within the article.

## Conflicts of Interest

The authors declare that they have no conflicts of interest.

## References

[1] T. S. Rappaport, Y. Xing, G. R. MacCartney, A. F. Molisch, E. Mellios, and J. Zhang, "Overview of millimeter wave communications for fifth-generation (5G) wireless networks—with a focus on propagation models," *IEEE Transactions on Antennas and Propagation*, vol. 65, no. 12, pp. 6213–6230, 2017.

[2] W. Hong, Z. H. Jiang, C. Yu et al., "Multibeam antenna technologies for 5G wireless communications," *IEEE Transactions on Antennas and Propagation*, vol. 65, no. 12, pp. 6231–6249, 2017.

[3] T. S. Rappaport, S. Sun, R. Mayzus et al., "Millimeter wave mobile communications for 5G cellular: it will work!," *IEEE Access*, vol. 1, pp. 335–349, 2013.

[4] O. M. Haraz, A. Elboushi, S. A. Alshebeili, and A.-R. Sebak, "Dense dielectric patch array antenna with improved radiation characteristics using EBG ground structure and dielectric superstrate for future 5G cellular networks," *IEEE Access*, vol. 2, pp. 909–913, 2014.

[5] W. T. Sethi, M. A. Ashraf, A. Ragheb, A. Alasaad, and S. A. Alshebeili, "Demonstration of millimeter wave 5G setup employing high-gain Vivaldi array," *International Journal of Antennas and Propagation*, vol. 2018, Article ID 3927153, 12 pages, 2018.

[6] J. Huang and J. Encinar, *Reflectarray Antennas*, Wiley-IEEE Press, 2008.

[7] M. H. Dahri, M. H. Jamaluddin, M. I. Abbasi, and M. R. Kamarudin, "A review of wideband reflectarray antennas for 5G communication systems," *IEEE Access*, vol. 5, pp. 17803–17815, 2017.

[8] S. V. Hum and J. Perruisseau-Carrier, "Reconfigurable reflectarrays and array lenses for dynamic antenna beam control: a review," *IEEE Transactions on Antennas and Propagation*, vol. 62, no. 1, pp. 183–198, 2014.

[9] F. Venneri, S. Costanzo, and G. Di Massa, "Design and validation of a reconfigurable single varactor-tuned reflectarray," *IEEE Transactions on Antennas and Propagation*, vol. 61, no. 2, pp. 635–645, 2013.

[10] S. Costanzo, F. Venneri, A. Raffo, G. Di Massa, and P. Corsonello, "Radial-shaped single varactor-tuned phasing line for active reflectarrays," *IEEE Transactions on Antennas and Propagation*, vol. 64, no. 7, pp. 3254–3259, 2016.

[11] S. Costanzo, F. Venneri, G. Di Massa, A. Borgia, and A. Raffo, "Bandwidth performances of reconfigurable reflectarrays: state of art and future challenges," *Radioengineering*, vol. 27, no. 1, pp. 1–9, 2018.

[12] S. Costanzo and F. Venneri, "Miniaturized fractal reflectarray element using fixed-size patch," *IEEE Antennas and Wireless Propagation Letters*, vol. 13, pp. 1437–1440, 2014.

[13] S. Costanzo, F. Venneri, G. Di Massa, A. Borgia, A. Costanzo, and A. Raffo, "Fractal reflectarray antennas: state of art and new opportunities," *International Journal of Antennas and Propagation*, vol. 2016, Article ID 7165143, 17 pages, 2016.

[14] K. H. Sayidmarie and M. E. Bialkowski, "Fractal unit cells of increased phasing range and low slopes for single-layer microstrip reflectarrays," *IET Microwaves, Antennas & Propagation*, vol. 5, no. 11, p. 1371, 2011.

[15] F. Xue, H. J. Wang, M. Yi, and G. Liu, "A broadband Ku-band microstrip reflectarray antenna using single-layer fractal elements," *Microwave and Optical Technology Letters*, vol. 58, no. 3, pp. 658–662, 2016.

[16] D. Oloumi, S. Ebadi, A. Kordzadeh, A. Semnani, P. Mousavi, and X. Gong, "Miniaturized reflectarray unit cell using fractal-shaped patch-slot configuration," *IEEE Antennas and Wireless Propagation Letters*, vol. 11, pp. 10–13, 2012.

[17] M. R. Chaharmir, J. Shaker, and H. Legay, "Dual-band Ka/X reflectarray with broadband loop elements," *IET Microwaves, Antennas & Propagation*, vol. 4, no. 2, pp. 225–231, 2010.

[18] Y. Pan, Y. R. Zhang, and X. Yu, "A X/Ku dual-band reflectarray design with cosecant squared shaped beam," *Microwave and Optical Technology Letters*, vol. 56, no. 9, pp. 2028–2034, 2014.

[19] Z. Hamzavi-Zarghani and Z. Atlasbaf, "A new broadband single-layer dual-band reflectarray antenna in X- and Ku-bands," *IEEE Antennas and Wireless Propagation Letters*, vol. 14, pp. 602–605, 2015.

[20] R. S. Malfajani and Z. Atlasbaf, "Design and implementation of a dual-band single layer reflectarray in X and K bands," *IEEE Transactions on Antennas and Propagation*, vol. 62, no. 8, pp. 4425–4431, 2014.

[21] S. W. Qu, Q. Y. Chen, M. Y. Xia, and X. Y. Zhang, "Single-layer dual-band reflectarray with single linear polarization," *IEEE Transactions on Antennas and Propagation*, vol. 62, no. 1, pp. 199–205, 2014.

[22] C. A. Balanis, *Antenna Theory Analysis and Design*, Wiley, New York, NY, USA, 1989.

[23] S. Costanzo, I. Venneri, G. Massa, and A. Borgia, "Benzocyclobutene as substrate material for planar millimeter-wave structures: dielectric characterization and application," *Journal of Infrared, Millimeter, and Terahertz Waves*, vol. 31, p. 66, 2010.

[24] S. Costanzo, F. Venneri, A. Borgia, I. Venneri, and G. Di Massa, "60 GHz microstrip reflectarray on a benzocyclobutene dielectric substrate," *IET Science, Measurement and Technology*, vol. 5, no. 4, pp. 134–139, 2011.

[25] "Ansoft Designer®," https://www.ansys.com.

[26] D. M. Pozar, S. D. Targonski, and H. D. Syrigos, "Design of millimeter wave microstrip reflectarrays," *IEEE Transactions on Antennas and Propagation*, vol. 45, no. 2, pp. 287–296, 1997.

[27] https://www.rogerscorp.com.

[28] "LPKF ProtoMat," https://www.lpkf.com/.